Nanoscale

PAPER

View Article Online
View Journal | View Issue

Cite this: *Nanoscale*, 2023, **15**, 11707

Strong light–matter coupling in pentacene thin films on plasmonic arrays†

Christoph P. Theurer,[a] Florian Laible,[a] Jia Tang,[a] Katharina Broch,[a,b] Monika Fleischer *[a,b] and Frank Schreiber *[a,b]

Received 9th March 2023,
Accepted 18th June 2023

DOI: 10.1039/d3nr01108a

rsc.li/nanoscale

Utilizing strong light–matter coupling is an elegant and powerful way to modify the energy landscapes of excited states of organic semiconductors. Consequently, the chemical and photophysical properties of these organic semiconductors can be influenced without the need of chemical modification but simply by implementing them in optical microcavities. This has so far mostly been shown in Fabry–Pérot cavities and with organic single crystals or diluted molecules in a host matrix. Here, we demonstrate strong, simultaneous coupling of the two Davydov transitions in polycrystalline pentacene thin films to surface lattice resonances supported by open cavities made of silver nanoparticle arrays. Such thin films are more easily fabricated and, together with the open architecture, more suitable for device applications.

1. Introduction

Strong light–matter coupling in organic semiconductors in microcavities leads to the formation of quasi-particles, consisting of photonic and excitonic contributions, called exciton-polaritons.[1,2] They were shown in recent years to feature fascinating effects like an enhancement of the exciton diffusion length, polariton lasing or quantum condensation with a wealth of possible applications.[3–7] Most studies focused so far on Fabry–Pérot microcavities, consisting of a pair of mirrors in between which the organic material is placed, which limits the possibilities for accessing the organic layer.[7,8] In contrast, open cavities of nanoparticles allow for an easy in- and out-coupling of light and exhibit an easily accessible surface for material deposition and contacting (Fig. 1a), which explains the increasing interest in recent years.[9–15] While single nanoparticles show relatively broad localized surface plasmon resonances (LSPRs), which have found application, *e.g.*, in biosensors,[16–18] periodic lattices of nanoparticles can support surface lattice resonances (SLRs) with much higher quality factors and delocalization of the electric field.[19–21] The quality factor can hereby be estimated as $Q = \lambda_m/\Delta\lambda$, with λ_m being the resonance wavelength and $\Delta\lambda$ the width of the resonance, which is linked to the energy loss of the oscillator.[20] A SLR results from the far-field dipole coupling of plasmonic nanoparticles in a periodic array (Fig. 1a), if the scattered light from neighboring particles arrives in phase with the illuminating light.[20] This condition is met close to diffraction edges (or Rayleigh anomalies), where a diffraction of the incident light into the plane of the array is found.[22] With a certain detuning between the diffraction edge and the LSPR of the single particles, strong and sharp SLRs can be realized.[23] Since the electric field of these SLRs is more delocalized in between the particles, a larger fraction of molecules can couple to this cavity field compared to the strongly localized near-field of the LSPRs of the single particles.

These properties make arrays of nanoparticles especially interesting for the investigation of strong light–matter coupling with organic semiconductors (Fig. 1b).[25–30] By strong coupling, the energy landscapes of the excited states of organic semiconductors can be modified by the formation of polariton bands at energies higher and lower than the pure exciton energy, which in turn influences the photophysical processes.[31,32] One such process that attracted appreciable interest in the last decade is singlet fission (SF), which describes the spontaneous splitting of one excited singlet exciton into two triplet excitons *via* a triplet pair state.[33,34] This SF process finds potential application in solar cells due to the duplication of the number of excitons.[35,36] Since the energy balance between the initial singlet state and the two triplet states is one major criterion for SF, this process is expected to be significantly influenced by strong light–matter coupling (Fig. 2).[24,37,38] However, experimental reports about the realization of strong coupling in SF materials are scarce and mainly stem from closed cavities.[11,39,40] Furthermore, investigations

---

[a] *Institut für Angewandte Physik, Universität Tübingen, Auf der Morgenstelle 10, 72076 Tübingen, Germany. E-mail: monika.fleischer@uni-tuebingen.de, frank.schreiber@uni-tuebingen.de*

[b] *Center for Light-Matter Interaction, Sensors & Analytics (LISA$^+$), Universität Tübingen, Auf der Morgenstelle 15, 72076 Tübingen, Germany*

† Electronic supplementary information (ESI) available: Details on plasmonic arrays with different geometries and additional extinction spectra. See DOI: **https://doi.org/10.1039/d3nr01108a**

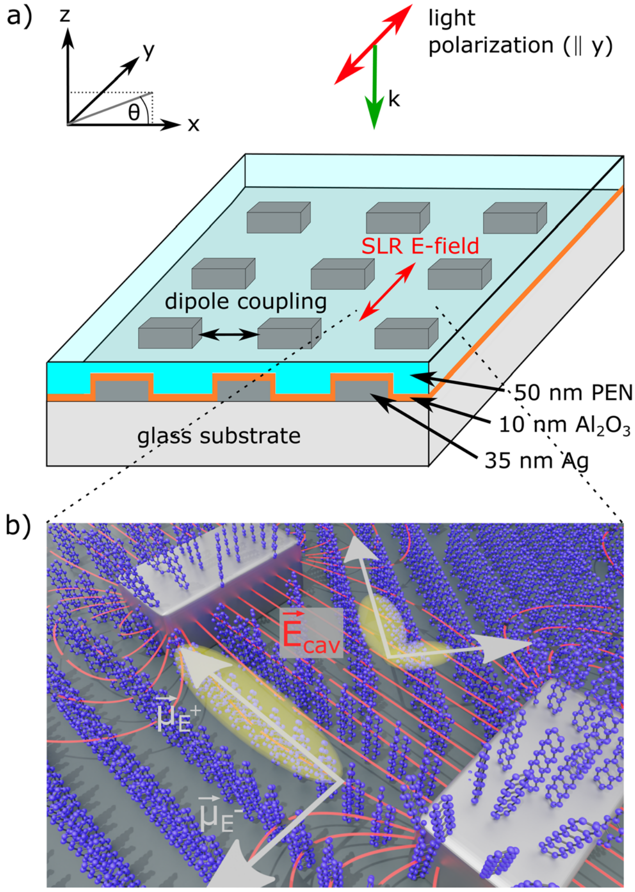

Fig. 1 (a) Scheme of the sample structure and the important orientations. The 2 nm thick titanium adhesion layer below the silver structures was omitted for clarity. The red and green arrows indicate the direction of polarization (along *y*) and propagation (along -*z*) of the illumination light and θ the rotation angle of the sample around the *y*-axis. (b) Graphical illustration of the coupling between differently oriented PEN crystallites (blue) and the SLR resulting from the silver nanorods (electric field indicated by red lines). The gray arrows indicate the in-plane transition dipole moments (TDMs) of the two Davydov components (DCs) and the size of the yellow halo the coupling strength.

on coupling in polycrystalline thin films are in general very rare due to the additional interfering parameters of intermolecular interactions and disorder.[41] Yet, for device applications thin films are of major importance.[42]

In this work, we used pentacene (PEN) thin films as organic material on open nanoparticle cavities, since PEN is a prototypical organic semiconductor and SF material.[36,43,44] It exhibits very fast, exothermic SF involving most likely a vibrationally excited triplet pair state to match the energy of the singlet state.[45,46] The modification of the SF process in PEN by strong light–matter coupling has been recently theoretically investigated.[24,38] By the coupling, the energy of the initial state is modified, which is now the lower polariton band (Fig. 2). Depending on the coupling strength, three different scenarios are possible. The lower polariton band might be energetically (i) in resonance with the triplet pair state dressed by another vibration, (ii) in resonance with the vibrationally relaxed triplet pair state, or, (iii) below the vibrationally relaxed triplet pair state. This should influence the triplet pair formation rate and could potentially render the reverse process of triplet fusion possible. However, to the authors' knowledge, so far there is only one experimental investigation of the coupling of PEN to surface plasmons in silver nanohole films,[47] and one of 6,13-bis(triisopropylsilylethynyl)pentacene dissolved in polystyrene in a closed cavity.[40]

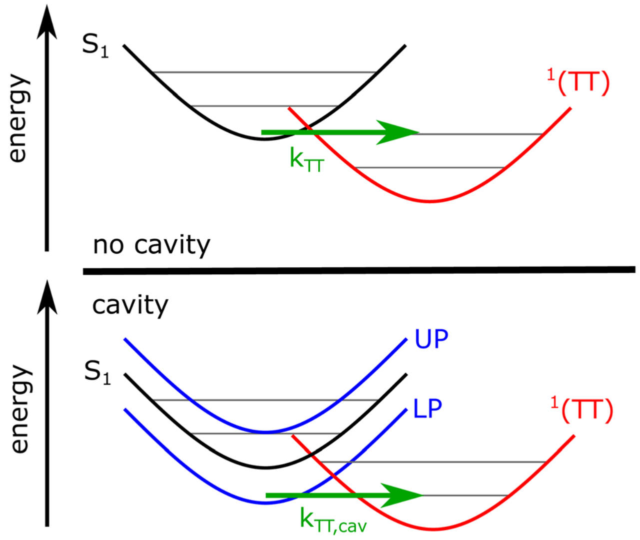

Fig. 2 Schematic energy levels of the SF process, without and with coupling to a cavity photon. S_1, ^{1}(TT), UP, LP, and $k_{TT}/k_{TT,cav}$ denote the PEN singlet (the lower DC) and triplet pair states, the upper and lower polariton, and the triplet pair formation rate outside/inside the cavity, respectively. Inspired by ref. 24.

2. Experimental

Plasmonic nanoantenna arrays were prepared by electron-beam lithography and metal deposition (see ESI† for details). Cleaned glass coverslips were used as the substrate, and a ∼2 nm thick titanium layer was deposited as an adhesion layer. The antennas consist of silver with a thickness of 35 nm (±10%). Different sample types were produced for comparison, namely rectangular arrays of rods, square arrays of discs, and samples with randomly arranged rods and discs (see ESI† for details). The standard deviation of the distances between particles within an array is below 3% as determined from scanning electron microscope (SEM) images. The standard deviation of the diameter d of the discs and the width w and length s of the rods within an array was determined to be below 7%, 10%, and 3%, respectively. To protect the silver structures from degradation in air or by the following processing steps, a 10 nm thick Al_2O_3 layer, homogeneously covering the whole surface, was consequently added *via* atomic layer deposition.

For the measurement of the arrays without coupling effects to molecules, a ∼140 nm thick reference layer of polystyrene (PS) was spin-coated (60 s at 2500 rpm) from a toluene solution

(~2.5 wt%) onto the samples to match the refractive index of PEN. For the measurements of the coupled PEN/plasmonic array systems, the reference layer was removed in toluene and a PEN (99.995% purity, Sigma-Aldrich) layer was applied *via* organic molecular beam deposition. This was done in a vacuum chamber with a base pressure of 2×10^{-8} mbar at a growth rate of 6 Å min^{-1}. The final PEN thickness was 50 ± 5 nm.

Transmission measurements were performed on an inverse Nikon (Eclipse 80i) microscope coupled to a grating spectrometer (LOT SR-303i-B). The transmitted light was collected by a 20 × objective with a numerical aperture of 0.45 and directed to the 100 μm entrance slit of the spectrometer, leading to a spectroscopically analyzed area of $5 \times 5\ \mu\text{m}^2$. The samples were illuminated from the top by collimated light from a halogen lamp. A rotatable polarizer can be inserted in the illumination path. Additionally to the transmitted intensity measured at the array/area of interest I_raw, the transmitted intensity beside the array/area of interest was measured as background I_BG. Finally, also a spectrum without illumination (dark current) I_dark was taken. The final, background corrected extinction *Ex* was calculated by

$$E_x = \frac{I_\text{BG} - I_\text{raw}}{I_\text{BG} - I_\text{dark}}. \tag{1}$$

3. Results and discussion

We used polycrystalline PEN thin films as organic, excitonic material in this work. The extinction spectrum of a neat PEN thin film is shown in Fig. 3a and exhibits a Davydov splitting of the lowest-energy exciton transition with the two Davydov components (DCs) denoted as E^+ and E^-.[48,49] The Davydov splitting results from the two translationally inequivalent molecules in the unit cell, and E^+ and E^- are polarized perpendicular to each other and have different oscillator strengths.[48,49] The polarization, given by the direction of the transition dipole moment (TDM) $\vec{\mu}$, as well as the oscillator strength, which is connected to $|\vec{\mu}|$, determine the strength of the light–matter coupling for the two DCs in the cavity field $\vec{E}_\text{cav}$ (Fig. 1b). The cavity field is provided by the SLR of the nanoparticle array, as demonstrated by the simulations presented in the ESI.† For PEN thin films, the TDMs of the two DCs lie almost perfectly in the plane of the substrate,[48,50] see ESI† for details. Due to the random orientation of the crystallites in the substrate plane[51,52] and the relatively large probing spot size ($5 \times 5\ \mu\text{m}^2$), an effective, averaged coupling strength for each DC is obtained by the extinction measurements of the coupled systems discussed below.[53] Quantitatively, the collective coupling strength $\hbar g_N$ within the dipole approximation and its connection to the experimentally accessible Rabi splitting $\hbar\Omega$ is given by[54]

$$\hbar\Omega = 2\hbar g_N = 2\sqrt{N}\vec{\mu}\cdot\vec{E}_\text{cav} = 2\vec{\mu}\cdot\hat{e}_\text{cav}\sqrt{\frac{N\hbar\omega_\text{exc}}{2\varepsilon_\text{r}\varepsilon_0 V}}, \tag{2}$$

where N denotes the number of coupled unit cells, $\hbar\omega_\text{exc}$ the exciton energy, V the cavity mode volume, ε_0 the vacuum permittivity, and $\hat{e}_\text{cav}$ a unitary vector in the direction of the cavity electric field. The relative permittivity of the organic layer is denoted by ε_r.[55] Strong coupling is achieved if the Rabi splitting is larger than the mean of the losses, approximated by the linewidths of the resonances.[54,56] The electric field enhancement by the SLR and the small linewidth of this resonance are therefore critical to achieve strong coupling.

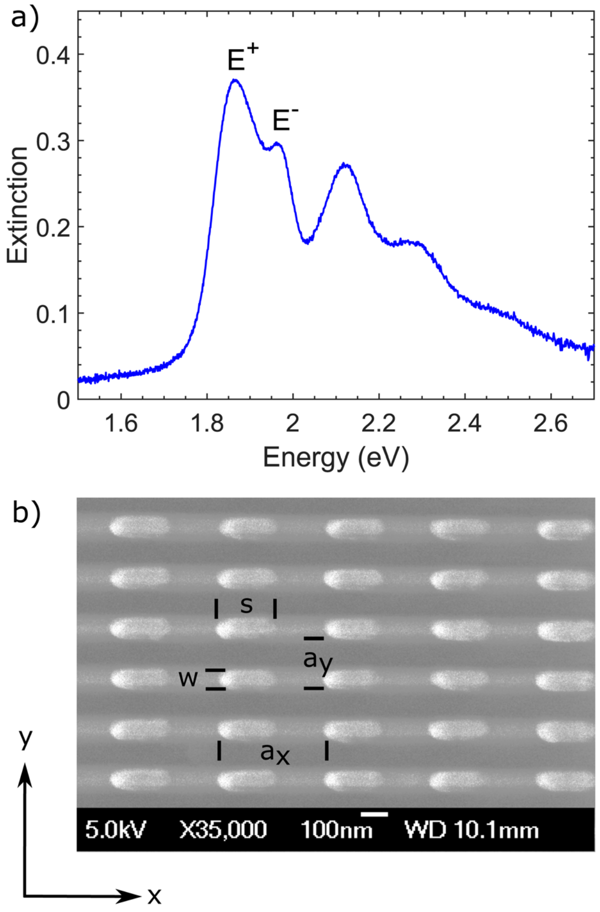

Fig. 3 (a) Extinction spectrum of a 50 nm thick PEN film on an Al_2O_3 layer on glass with the two Davydov components E^+ and E^-. (b) SEM image of an array of silver nanorods on glass, with a covering layer of Al_2O_3 over the entire surface. The lattice parameters a_x and a_y and the single structure dimensions *s* and *w* are indicated.

As the inorganic cavity, $25 \times 25\ \mu\text{m}^2$ large arrays of silver nanoparticles were used. They offer the advantages of having an openly accessible surface for the PEN thin film deposition and a low internal damping in the silver particles at optical frequencies.[57] The parameters of the arrays, namely the particle size and shape, as well as the lattice constants, were experimentally adjusted to obtain arrays with strong and sharp SLRs at the energy of E^+, since this is the lowest energy transition in PEN with critical importance for the SF process.[45] These criteria were best met by rectangular arrays of nanorods (Fig. 3b) with width w = 85 ± 8 nm, length s = 200 ± 5 nm, and lattice constants a_x = 415 ± 9 nm and a_y = 190 ± 5 nm, determined from SEM images. The given deviations are statistical variations within one array. Under y-polarized excitation (Fig. 1a), the small width of the rods leads to a LSPR at high energies (~2.5 eV), and the lattice constant a_x leads to a diffraction edge just above the energy of E^+, resulting in a sharp SLR at the energy of E^+. The larger length s of the rods and the smaller lattice constant a_y enhance the overall SLR strength,[23] which is confirmed by the comparison to square arrays of nanodiscs, see ESI.† On top of the silver structures and the whole surface, a 10 nm thick aluminum oxide (Al_2O_3) protection layer was introduced *via* atomic layer deposition to avoid degradation of the nanostructures and direct electron transfer between PEN and the silver structures. A scheme of the samples is shown in Fig. 1a and exemplary SEM images in Fig. 3b and Fig. S1 in the ESI.†

First, the extinction spectra of the bare arrays were taken as reference to confirm the energy position of the SLRs. To match the refractive index of PEN ($n \approx 1.6$ at frequencies other than the exciton transition frequencies[52]) in the reference measurements, a PS film with a thickness of ~140 nm was used as reference layer owing to its refractive index of $n = 1.59$. This similar refractive index is crucial for meaningful reference measurements due to its influence on the energy position of the LSPR and SLR. Furthermore, SLRs are only observable if the difference in the refractive index between the substrate and the medium above is not too large, which would be the case for air.[19,58] All spectra were referenced to the signal measured beside the array for background correction as described above. All spectra were taken under y-polarized excitation (Fig. 1a), hence excitation along the short axis of the rods. The extinction of one exemplary rod array is shown in Fig. 4, while spectra of further rod arrays are shown in Fig. S5 in the ESI.† The extinction spectra under normal illumination exhibit one sharp SLR peak around the energy of the two DCs of PEN. Owing to the slightly different chosen rod dimensions (see ESI†), the different rod arrays exhibit slightly differing SLR strengths (extinction between 0.6 and 0.8), quality factors (25–40, determined by Lorentzian fits), and resonance energies (1.85 eV–1.89 eV). The square arrays of discs exhibit similar extinction spectra (see Fig. S7 in the ESI†), but with smaller strengths and quality factors due to smaller particles and smaller detuning between the LSPR and the diffraction edge.[59]

Upon rotation of the sample around the y-axis by $\theta = 3°$ or $\theta = 6°$ (Fig. 1a) and hence transversal electric (TE) illumination with a wave vector component along the long nanorod axis, the SLR splits into two, following the (1, 0) and (−1, 0) diffraction edges as expected. Here, the lower energy SLR has a smaller width due to the larger detuning from the LSPR, which is more strongly pronounced in the disc spectra. The wavelengths of the diffraction edges, which are also included in Fig. 4, are given by[20]

$$\lambda_{\pm 1} = a_x(n_{\text{eff}} \pm \sin\theta), \tag{3}$$

with an empirically determined, effective refractive index $n_{\text{eff}} = 1.53$ between the ones of the glass substrate and the PS layer. By the rotation, the SLRs of the arrays can be shifted out of resonance with respect to the PEN transitions.

To study the light–matter coupling, the PS layer was removed from the arrays and replaced by a 50 nm thick PEN film *via* organic molecular beam deposition. The extinction spectra of the resulting coupled systems are shown in Fig. 5 and Fig. S6 and S8 in the ESI.† Under normal illumination, a clear change in the spectrum is observed, with now three peaks instead of one SLR. They are labeled in Fig. 5 by A, B, and C and are assigned to three polariton bands that result

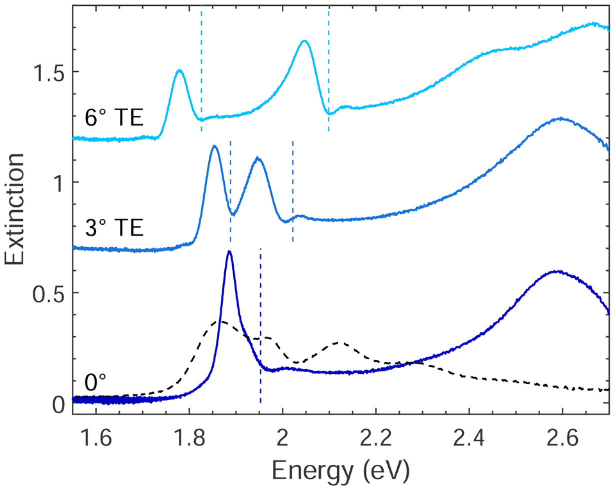

Fig. 4 Extinction spectra of a plasmonic array covered by a polystyrene reference film. The dimensions of the lattice and rods are a_x = 415 nm, a_y = 190 nm, s = 200 nm, w = 85 nm, and h = 35 nm. The spectra taken under θ = 3° and θ = 6° are vertically offset for clarity. The black dashed spectrum is the extinction spectrum of a PEN thin film for peak position comparison. The dashed vertical lines indicate the (1, 0) and (−1, 0) diffraction edges.

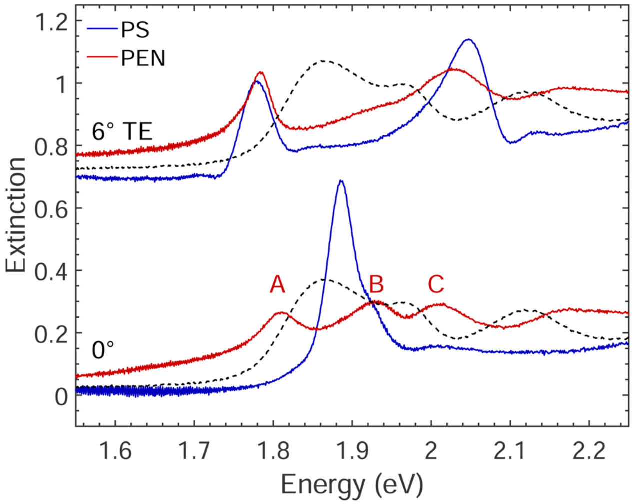

Fig. 5 Extinction spectra of the same plasmonic array as in Fig. 4 (a_x = 415 nm, a_y = 190 nm, s = 200 nm, w = 85 nm, h = 35 nm), covered by a 50 nm PEN film (red) and the PS film for reference (blue). The spectra obtained under θ = 6° TE illumination are vertically offset for clarity. The black dotted line is the extinction spectrum of the PEN thin film recorded beside the array for peak position comparison.

from the coupling of the array SLR with the two Davydov transitions of PEN, in accordance to the assignment in similar systems.[60,61] The splitting between the lower polariton band A and the middle one, B, can hereby mainly be attributed to coupling of the SLR with E^+, while the splitting between B and C may be attributed to coupling between the SLR and E^-.[62] While this is only an approximation and the respectively other DC as well as the first vibronic transition will also contribute to the coupling,[63] the larger splitting between A and B compared to B and C is nicely consistent with the larger TDM for E^+ (μ = 5.76 D) compared to E^- (μ = 3.53 D).[50]

If we next consider the extinction spectra of the arrays with PEN under an illumination angle of $\theta = 6°$, the peak positions are nearly identical to the ones with the PS reference layer. This indicates that this rotation is already sufficient to move the SLRs far enough out of resonance with E^+ and E^- that the coupling to the molecular transitions does not have a significant influence on the SLR resonance energies. The slight shift of the upper SLR probably results from influences of the first vibronic transition. This possibility to shift the SLRs out of resonance with E^+ is of importance for studies of the influence of the polariton formation on the photophysics in the coupled PEN array system, since it allows to remove the effects by a rotation of the sample. Thus, reference measurements at the exact same position of a sample can be taken. This might be exploited in transient absorption experiments to characterize the influence of polariton formation on the SF time constants by pumping and probing under changing angles. In passing, it can additionally be mentioned that the spectra under $\theta = 6°$ confirm that the refractive indices of PS and PEN are similar and that the performed background subtraction works well, since no PEN features appear.

The averaged visible collective coupling strength between the SLR and the two DCs was approximated from the splitting of the A and B, and the B and C polariton band, respectively, under normal illumination (Fig. 5 and Fig. S6 in the ESI†), since here the resonance detuning is minimal. From the shown four different rod arrays energy differences corresponding to a Rabi splitting of 120 meV and 80–90 meV between the A and B and B and C polariton peaks, respectively, were found. The linewidths (FWHM) of the two DCs were fitted by Gaussians to $\gamma_{E^+} \approx$ 120 meV and $\gamma_{E^-} \approx$ 90 meV, respectively. The linewidths of the SLRs of the different arrays, corresponding to their losses, are determined by Lorentzian fits to 55 meV $\leq \gamma_{\mathrm{SLR}} \leq$ 75 meV.

With the definition that strong coupling is realized if the Rabi splitting is larger than the mean linewidth $\gamma_{\mathrm{m}} = (\gamma_{\mathrm{E}} + \gamma_{\mathrm{SLR}})/2$ of the resonances,[56,60] the coupling between E^+ and the SLR can be categorized as strong while the one to E^- is in the regime between strong and weak coupling. The collective coupling strength results in $\hbar g_{N,E^+} \approx$ 60 meV and $\hbar g_{N,E^-} \approx$ 40 meV (eqn (2)). The ratio of 1.5 between them meets the expectations based on the ratio of 1.6 between their TDMs.[50]

The obtained splitting should be understood as an averaged, lower bound for the coupling strength, since we measured polycrystalline films without a perfect alignment of the TDMs with respect to the cavity field. Since the two DCs are polarized orthogonal to each other, at most one of them could be aligned in the direction of the field. Hence, the spectra are averages over all different relative orientations. Based on the similarity of the extinction spectrum of the PEN film recorded next to an array and on a non-coupling array (Fig. S11†), we conclude on a similar molecular orientation, namely nearly upright-standing on the substrate (see ESI† for details).[64] Thus, the TDMs of the two DCs lie in the plane of the substrate, and the averaged measured splitting value corresponds to ~64% of the maximal value at perfect alignment (eqn (2)). If in close proximity to the silver structures a completely random orientation would be assumed, due to the uneven substrate, the measured value would even be only ~41% of the maximal value.

We can also theoretically approximate the maximal coupling strength by eqn (2). Under the assumption that the entire mode volume is filled with PEN molecules, the $\frac{N}{V}$ term corresponds to the unit cell density in the PEN (thin film) crystal structure,[64] which is $\rho_{\mathrm{uc}} = 1.43 \times 10^{27}\ \mathrm{m}^{-3}$. Furthermore, the transition energy $\hbar\omega_{E^+}$ = 1.86 eV of the lower DC is known, as well as its absolute TDM μ_{E^+} = 5.76 D.[50] Due to the anisotropy of the PEN thin films, the polarizability depends on the crystal direction, resulting in a relative permittivity tensor.[65] In the plane of the substrate, an averaged relative permittivity of $\varepsilon_{\mathrm{r}} \sim 3$ is assumed.[65] With these values, a maximal theoretical collective coupling strength of $\hbar g_{N,E^+,\mathrm{theo}} \approx$ 340 meV can be calculated. This value is much larger than the experimentally observed one ($\hbar g_{N,E^+} \approx$ 60 meV), which can partially be explained by the averaging due to the polycrystalline thin film. Another important factor that reduces the experimental value is that not the entire mode volume can be filled by PEN molecules, since it also extends into the glass substrate and the Al_2O_3 protection layer. The extension of the mode volume is illustrated by simulations of the electric field of the SLR, which are presented in the ESI.† Thus, the number of coupled molecules and hence the collective coupling strength is reduced. This overall underlines the promising coupling capabilities of the low-energy PEN transitions.

4. Conclusions

Taken together, due to the strong TDM of the lower DC E^+ in PEN, strong coupling to SLRs in arrays of silver nanorods was realized in polycrystalline PEN thin films. Simultaneously, also the interaction of the upper DC E^- and the SLR of the array is close to the strong coupling limit. The strong coupling leads to a lower polariton band around 1.80 eV, hence ~60 meV lower than the lowest transition in PEN without coupling at 1.86 eV. The coupling of the triplet pair state, as intermediate in the SF process, to the SLR should be negligible due to its vanishing TDM.[24,38] This implies that the energy gap to the triplet pair state, with an energy of approximately 1.65–1.7 eV, is significantly reduced, but the overall SF process remains exothermic.[44] A measurement of the resulting changes in the SF rate would be an interesting follow-up experiment to our study, in particular to establish an alternative measure to tune SF rates without chemical modifications.

Author contributions

C. P. T. and J. T. prepared the samples. C. P. T. and F. L. performed and evaluated the experiments. F. L. performed the simulations. K. B., M. F., and F. S. conceived and supervised the project. C. P. T. wrote the manuscript with input from all authors. All authors gave approval to the final version of the manuscript.

Conflicts of interest

There are no conflicts to declare.

Acknowledgements

The authors thank Dr. Anke Horneber for assistance during the measurements. The authors gratefully acknowledge funding by the German Research Foundation (DFG) through the projects FL 670/8-1, BR 4869/4-1, and SCHR 700/20-2. F. L. gratefully acknowledges funding by the Vector-Stiftung through the project 2021-0129.

References

1 D. G. Lidzey, D. D. C. Bradley, M. S. Skolnick, T. Virgili, S. Walker and D. M. Whittaker, *Nature*, 1998, **395**, 53–55.

2 P. Törmä and W. L. Barnes, *Rep. Prog. Phys.*, 2015, **78**, 013901.

3 J. Schachenmayer, C. Genes, E. Tignone and G. Pupillo, *Phys. Rev. Lett.*, 2015, **114**, 196403.

4 S. Kéna-Cohen and S. Forrest, *Nat. Photonics*, 2010, **4**, 371–375.

5 J. D. Plumhof, T. Stöferle, L. Mai, U. Scherf and R. F. Mahrt, *Nat. Mater.*, 2014, **13**, 247–252.

6 A. V. Zasedatelev, A. V. Baranikov, D. Urbonas, F. Scafirimuto, U. Scherf, T. Stöferle, R. F. Mahrt and P. G. Lagoudakis, *Nat. Photonics*, 2019, **13**, 378–383.

7 D. Sanvitto and S. Kéna-Cohen, *Nat. Mater.*, 2016, **15**, 1061–1073.

8 D. Polak, R. Jayaprakash, T. P. Lyons, L. Á. Martínez-Martínez, A. Leventis, K. J. Fallon, H. Coulthard, D. G. Bossanyi, K. Georgiou, A. J. Petty, *et al.*, *Chem. Sci.*, 2020, **11**, 343–354.

9 M. Ramezani, A. Halpin, A. I. Fernández-Domínguez, J. Feist, S. R.-K. Rodriguez, F. J. Garcia-Vidal and J. G. Rivas, *Optica*, 2017, **4**, 31–37.

10 A. I. Väkeväinen, R. J. Moerland, H. T. Rekola, A.-P. Eskelinen, J.-P. Martikainen, D.-H. Kim and P. Törmä, *Nano Lett.*, 2014, **14**, 1721–1727.

11 A. M. Berghuis, A. Halpin, Q. Le-Van, M. Ramezani, S. Wang, S. Murai and J. Gómez Rivas, *Adv. Funct. Mater.*, 2019, **29**, 1901317.

12 D. A. Gollmer, C. Lorch, F. Schreiber, D. P. Kern and M. Fleischer, *Phys. Rev. Mater.*, 2017, **1**, 054602.

13 D. A. Gollmer, C. Lorch, F. Schreiber, D. P. Kern and M. Fleischer, *J. Opt. Soc. Am. B*, 2019, **36**, E9–E14.

14 R. Guo, S. Derom, A. I. Väkeväinen, R. J. A. van Dijk-Moes, P. Liljeroth, D. Vanmaekelbergh and P. Törmä, *Opt. Express*, 2015, **23**, 28206–28215.

15 T. K. Hakala, H. T. Rekola, A. I. Väkeväinen, J.-P. Martikainen, M. Nečada, A. J. Moilanen and P. Törmä, *Nat. Commun.*, 2017, **8**, 13687.

16 J. R. Mejía-Salazar and O. N. Oliveira, *Chem. Rev.*, 2018, **118**, 10617–10625.

17 Y.-T. Long and C. Jing, *Localized Surface Plasmon Resonance Based Nanobiosensors*, Springer Berlin, Heidelberg, 2014.

18 F. Laible, A. Horneber and M. Fleischer, in *Optical Nanospectroscopy: Applications*, ed. A. J. Meixner, M. Fleischer, D. P. Kern, E. Sheremet and N. McMillan, Walter de Gruyter GmbH, Berlin/Boston, 2023, ch. 3.1.

19 B. Auguié and W. L. Barnes, *Phys. Rev. Lett.*, 2008, **101**, 143902.

20 V. G. Kravets, A. V. Kabashin, W. L. Barnes and A. N. Grigorenko, *Chem. Rev.*, 2018, **118**, 5912–5951.

21 A. D. Utyushev, V. I. Zakomirnyi and I. L. Rasskazov, *Rev. Phys.*, 2021, **6**, 100051.

22 A. G. Nikitin, A. V. Kabashin and H. Dallaporta, *Opt. Express*, 2012, **20**, 27941–27952.

23 M. B. Ross, C. A. Mirkin and G. C. Schatz, *J. Phys. Chem. C*, 2016, **120**, 816–830.

24 L. A. Martínez-Martínez, M. Du, R. F. Ribeiro, S. Kéna-Cohen and J. Yuen-Zhou, *J. Phys. Chem. Lett.*, 2018, **9**, 1951–1957.

25 W. Wang, M. Ramezani, A. I. Väkeväinen, P. Törmä, J. G. Rivas and T. W. Odom, *Mater. Today*, 2018, **21**, 303–314.

26 S. R. K. Rodriguez, J. Feist, M. A. Verschuuren, F. J. Garcia Vidal and J. Gómez Rivas, *Phys. Rev. Lett.*, 2013, **111**, 166802.

27 S. R. K. Rodriguez and J. G. Rivas, *Opt. Express*, 2013, **21**, 27411–27421.

28 L. Shi, T. K. Hakala, H. T. Rekola, J.-P. Martikainen, R. J. Moerland and P. Törmä, *Phys. Rev. Lett.*, 2014, **112**, 153002.

29 A. Yang, T. B. Hoang, M. Dridi, C. Deeb, M. H. Mikkelsen, G. C. Schatz and T. W. Odom, *Nat. Commun.*, 2015, **6**, 6939.

30 W. Zhou, M. Dridi, J. Y. Suh, C. H. Kim, D. T. Co, M. R. Wasielewski, G. C. Schatz and T. W. Odom, *Nat. Nanotechnol.*, 2013, **8**, 506–511.

31 A. Salomon, C. Genet and T. Ebbesen, *Angew. Chem., Int. Ed.*, 2009, **48**, 8748–8751.

32 P. Bai, S. ter Huurne, E. van Heijst, S. Murai and J. Gómez Rivas, *J. Chem. Phys.*, 2021, **154**, 134110.

33 M. B. Smith and J. Michl, *Chem. Rev.*, 2010, **110**, 6891–6936.

34 K. Miyata, F. S. Conrad-Burton, F. L. Geyer and X.-Y. Zhu, *Chem. Rev.*, 2019, **119**, 4261–4292.

35 M. K. Gish, N. A. Pace, G. Rumbles and J. C. Johnson, *J. Phys. Chem. C*, 2019, **123**, 3923–3934.

36 M. W. B. Wilson, A. Rao, B. Ehrler and R. H. Friend, *Acc. Chem. Res.*, 2013, **46**, 1330–1338.

37 B. Gu and S. Mukamel, *J. Phys. Chem. Lett.*, 2021, **12**, 2052–2056.

38 C. Climent, D. Casanova, J. Feist and F. J. Garcia-Vidal, *Cell Rep. Phys. Sci.*, 2022, **3**, 100841.

39 S. Takahashi, K. Watanabe and Y. Matsumoto, *J. Chem. Phys.*, 2019, **151**, 074703.

40 B. Liu, V. M. Menon and M. Y. Sfeir, *ACS Photonics*, 2020, **7**, 2292–2301.

41 M. Rödel, P. Lisinetskaya, M. Rudloff, T. Stark, J. Manara, R. Mitric and J. Pflaum, *J. Phys. Chem. C*, 2022, **126**, 4163–4171.

42 S. R. Forrest, *Nature*, 2004, **428**, 911–918.

43 M. E. Gershenson, V. Podzorov and A. F. Morpurgo, *Rev. Mod. Phys.*, 2006, **78**, 973–989.

44 C. K. Yong, A. J. Musser, S. L. Bayliss, S. Lukman, H. Tamura, O. Bubnova, R. K. Hallani, A. Meneau, R. Resel, M. Maruyama, *et al.*, *Nat. Commun.*, 2017, **8**, 15953.

45 A. A. Bakulin, S. E. Morgan, T. B. Kehoe, M. W. Wilson, A. W. Chin, D. Zigmantas, D. Egorova and A. Rao, *Nat. Chem.*, 2016, **8**, 16–23.

46 R. Tempelaar and D. R. Reichman, *J. Chem. Phys.*, 2018, **148**, 244701.

47 J. C. Johnson, T. H. Reilly, A. C. Kanarr and J. van de Lagemaat, *J. Phys. Chem. C*, 2009, **113**, 6871–6877.

48 I. Meyenburg, T. Breuer, A. Karthäuser, S. Chatterjee, G. Witte and W. Heimbrodt, *Phys. Chem. Chem. Phys.*, 2016, **18**, 3825–3831.

49 C. Cocchi, T. Breuer, G. Witte and C. Draxl, *Phys. Chem. Chem. Phys.*, 2018, **20**, 29724–29736.

50 T. Zeng, R. Hoffmann and N. Ananth, *J. Am. Chem. Soc.*, 2014, **136**, 5755–5764.

51 R. Ruiz, D. Choudhary, B. Nickel, T. Toccoli, K.-C. Chang, A. C. Mayer, P. Clancy, J. M. Blakely, R. L. Headrick, S. Iannotta and G. G. Malliaras, *Chem. Mater.*, 2004, **16**, 4497–4508.

52 A. Hinderhofer, U. Heinemeyer, A. Gerlach, S. Kowarik, R. M. J. Jacobs, Y. Sakamoto, T. Suzuki and F. Schreiber, *J. Chem. Phys.*, 2007, **127**, 194705.

53 H. L. Luk, J. Feist, J. J. Toppari and G. Groenhof, *J. Chem. Theory Comput.*, 2017, **13**, 4324–4335.

54 M. Hertzog, M. Wang, J. Mony and K. Börjesson, *Chem. Soc. Rev.*, 2019, **48**, 937–961.

55 R. Chikkaraddy, B. De Nijs, F. Benz, S. J. Barrow, O. A. Scherman, E. Rosta, A. Demetriadou, P. Fox, O. Hess and J. J. Baumberg, *Nature*, 2016, **535**, 127–130.

56 G. Khitrova, H. Gibbs, M. Kira, S. W. Koch and A. Scherer, *Nat. Phys.*, 2006, **2**, 81–90.

57 P. B. Johnson and R. W. Christy, *Phys. Rev. B: Solid State*, 1972, **6**, 4370–4379.

58 B. Auguié, X. M. Bendaña, W. L. Barnes and F. J. García de Abajo, *Phys. Rev. B: Condens. Matter Mater. Phys.*, 2010, **82**, 155447.

59 B. B. Rajeeva, L. Lin and Y. Zheng, *Nano Res.*, 2018, **11**, 4423–4440.

60 A. M. Berghuis, V. Serpenti, M. Ramezani, S. Wang and J. Gómez Rivas, *J. Phys. Chem. C*, 2020, **124**, 12030–12038.

61 M. Ramezani, Q. Le-Van, A. Halpin and J. Gómez Rivas, *Phys. Rev. Lett.*, 2018, **121**, 243904.

62 R. Deshmukh, P. Marques, A. Panda, M. Y. Sfeir, S. R. Forrest and V. M. Menon, *ACS Photonics*, 2020, **7**, 43–48.

63 M. Ramezani, A. Halpin, J. Feist, N. Van Hoof, A. I. Fernández-Domínguez, F. J. Garcia-Vidal and J. Gómez Rivas, *ACS Photonics*, 2018, **5**, 233–239.

64 S. Schiefer, M. Huth, A. Dobrinevski and B. Nickel, *J. Am. Chem. Soc.*, 2007, **129**, 10316–10317.

65 S. D. Ha, Y. Qi and A. Kahn, *Chem. Phys. Lett.*, 2010, **495**, 212–217.